DOI: 10.1002/chem.200600649

Deep Blue Mixed-Valent $Pt^{III}Pt^{III}Pt^{II}$ Complex $[Pt_3Br_2(\mu\text{-}pz)_6]$ (pz = Pyrazolate) Showing Valence-Detrapping Behavior in Solution

Keisuke Umakoshi,*[a] Takashi Kojima,[a] Yong Hun Kim,[a] Masayoshi Onishi,*[a] Yoshihide Nakao,[b] and Shigeyoshi Sakaki[b]

Abstract: The oxidation of the pyrazolate bridged cyclic Pt^{II} trimer, $[Pt_3(\mu\text{-}pz)_6]$ (**1**), in the presence of bromide ion gave a deep blue mixed-valent $Pt^{II,III,III}$ complex, $[Pt_3Br_2(\mu\text{-}pz)_6]$ (**2**). The structural analysis of **2** disclosed that the complex has localized Pt–Pt bond. Our theoretical calculations revealed that the HOMO and LUMO of $Pt_3^{II,III,III}$ species mainly consists of $(d_\sigma\text{–}d_\sigma)$ and $(d_\sigma\text{–}d_\sigma)^*$ orbitals, respectively, and the origin of deep blue color of the bromo complex, **2**, arises from the $(d_\sigma\text{–}d_\sigma)\rightarrow(d_\sigma\text{–}d_\sigma)^*$ transition. Unique fluxional behavior was observed due to valence-detrapping of **2** in solution. The activation parameters of the valence-detrapping of **2** obtained by Eyring analyses were $\Delta H^{\neq} = 37(2)\ \mathrm{kJ\,mol^{-1}}$ and $\Delta S^{\neq} = -67(7)\ \mathrm{J\,mol^{-1}\,K^{-1}}$.

Keywords: bridging ligands · fluxionality · metal–metal interactions · mixed-valent compounds · platinum

Introduction

Metal–metal bonded platinum complexes can be classified into two categories. One includes the complexes that have Pt–Pt bonds perpendicular to the square planes defined by coordinated atoms, such as Pt^{III} dimers,[1–4] linear mixed-valence complexes,[5–7] and one-dimensional complexes.[8,9] In such complexes, the d_{z^2} orbital of each Pt atom plays an important role in the formation of Pt–Pt bonds. The other includes the complexes consisting of the fragments with different geometries from the former category, such as acetato-bridged tetramers and trimers[10] and low-valent platinum clusters.[11] For these complexes, the contribution of the $d_{x^2-y^2}$ or p orbital becomes more dominant for the Pt–Pt bonds. Because most known cyclic trinuclear platinum clusters belong to the latter category, it is interesting and challenging to form direct Pt–Pt bonds by removing electrons mainly from d_{z^2} orbital of each Pt atom in the Pt^{II} trinuclear unit with face-to-face association,[12] which potentially belongs to the former category.

To synthesize such novel Pt–Pt bonds, the best-fit complex is probably the pyrazolato-bridged trinuclear platinum(II) complex, $[Pt_3(\mu\text{-}pz)_6]$ (pz = pyrazolate) (**1**), because it has very similar structure to a typical complex with face-to-face association, $[Pd_3(\mu\text{-}OAc)_6]$.[12,13] The complex **1** was originally prepared by Burger and Strähle in 1985,[14] and its convenient preparative route was recently developed by us.[15] To give an answer to the question about whether a direct Pt–Pt bond can be formed in the cyclic platinum trimer or not, we conducted the oxidation of **1** and succeeded, for the first time, in the isolation and characterization of the two-electron oxidized species, as well as the assignment of their electronic spectra. Very interestingly, the oxidized species show "valence-detrapping" behavior in solution. Here we define the term "valence-detrapped complexes" as the complexes that have sufficient energy to interconvert between their vibronic states faster than the NMR timescale.

It is known that the trinuclear mixed-valence complexes $[Fe_3(\mu\text{-}O)(\mu\text{-}O_2CCH_3)_6(L)_3]\cdot S$ (L = H_2O or (substituted) pyridine; S = solvate molecule), which can be described as trapped-valence $Fe^{III}{}_2Fe^{II}$ complexes on the 10^{-11}–10^{-12} s timescale at low temperatures, also start to interconvert between their three or four vibronic states as the crystal is heated.[16–18] In this case, an increase in temperature leads to a conversion from being valence trapped on the Mössbauer and NMR timescale to valence detrapped with accompany-

[a] Prof. Dr. K. Umakoshi, T. Kojima, Y. H. Kim, Prof. Dr. M. Onishi
Department of Applied Chemistry, Faculty of Engineering
Nagasaki University, Bunkyo-machi, Nagasaki 852–8521 (Japan)
Fax: (+81) 95-819-2672
E-mail: kumks@nagasaki-u.ac.jp
onishi@nagasaki-u.ac.jp

[b] Dr. Y. Nakao, Prof. Dr. S. Sakaki
Department of Molecular Engineering
Graduate School of Engineering, Kyoto University
Nishikyo-ku, Kyoto 615–8510 (Japan)

Supporting information for this article is available on the WWW under http://www.chemeurj.org/ or from the author.

ing phase transitions. According to the solid-state ^{2}H NMR studies, this conversion occurs together with an onset of motion of the S solvate molecule.[17] A theoretical model has also been developed to understand the effects of intermolecular interactions in the solid state upon the rate of intramolecular electron transfer.[19]

On the other hand, in the case of $[Pt_3Br_2(\mu\text{-}pz)_6]$, the valence-detrapping occurs in the solution state in associative manner, either through approach of solvent DMF molecule to the Br-coordinated Pt center or through approach of a Br^- ion to the uncoordinated Pt atom in the presence of excess Br^-. Herein we report on novel mixed-valent $Pt_3^{II,III,III}$ complexes, which belong to the trapped-valence system with the Pt–Pt d_σ bond perpendicular to the square planes and show intriguing valence-detrapping behavior in solution.

Results and Discussion

Synthesis, structure and properties of mixed-valence complex: The oxidation of **1** by $(NH_4)_2Ce^{IV}(NO_3)_6$ in the presence of KBr in CH_2Cl_2/H_2O afforded deep blue compound **2** irrespective of the complex/oxidizing agent ratio. The compound was found to be diamagnetic by the SQUID measurement, indicating that two-electron oxidation of **1** proceeded to give $Pt_3^{II,III,III}$ species with a singlet spin state. Single crystals of **2** were obtained by the recrystallization from $CHBr_3$. The X-ray structural analysis of **2** disclosed that the compound consists of discrete trinuclear Pt complex with bromo ligands at the axial site of two of the three platinum atoms and should be formulated as $[Pt_3Br_2(\mu\text{-}pz)_6]$ (Figure 1). The isosceles triangle complex molecule **2** has a crystallographically imposed twofold axis passing through the Pt2 atom and the midpoint of Pt1–Pt1* bond. The Pt1–Pt1* and Pt1···Pt2 distances are 2.7787(8) and 3.1267(5) Å, respectively; the former is 0.27 Å shorter and the latter is 0.08 Å longer than the average Pt···Pt distance (3.048 Å) in $[Pt_3(\mu\text{-}pz)_6]$,[14] which is an ideal equilateral triangle. This observation strongly indicates that the oxidation states of Pt1, Pt1*, and Pt2 atoms are +3, +3 and +2, respectively, and that the Pt–Pt single bond is localized between Pt1 and Pt1* atoms, which will be discussed below in more detail.

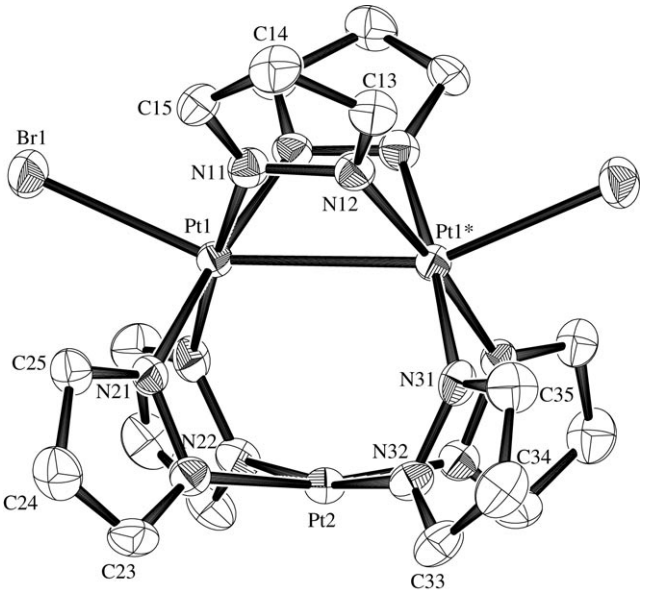

Figure 1. Molecular structure of **2** with the atomic labeling scheme (50% probability ellipsoids). Selected bond lengths [Å] and angles [°]: Pt1–Pt1*, 2.7787(8); Pt1···Pt2, 3.1267(5); Pt1–Br1, 2.584(1); Pt1*-Pt1-Pt2, 63.618(8); Pt1-Pt2-Pt1*, 52.76(2); Pt1*-Pt1-Br1, 156.40(2); Pt1*-Pt1-N11, 69.1(2); Pt1*-Pt1-N12*, 69.4(2); Pt2-Pt1-N21, 62.1(2); Pt2-Pt1-N31*, 61.8(2).

Similarly to the reactivity of dinuclear Pt^{III} complexes,[1,3–5,7] the axial bromo ligands at Pt^{III} sites in **2** can be replaced by chloro ligands to give purple complex $[Pt_3Cl_2(\mu\text{-}pz)_6]$ (**3**). The complex **3** can also be obtained by the oxidation of **1** in the presence of KCl instead of KBr. However, the instability of **3** in common organic solvents except for carbon tetrachloride and the contamination of **1** prevent from the full characterization of **3**. The UV/Vis spectra of **2** in DMF show three intense absorption bands at 16900, 21000, and 30600 cm^{-1} (Figure 2). The chloro complex **3** exhibits higher energy shift of the corresponding absorption bands at 18200, 22500, and 32800 cm^{-1}, respectively (Figure S6 in the Supporting Information).

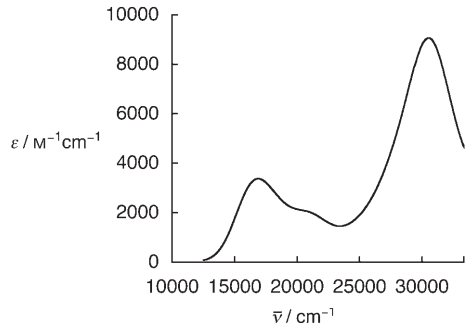

Figure 2. UV/Vis spectra of **2** in DMF: $\lambda_{max}(\varepsilon)$: 16900 (3400), 21000 (1800), 30600 cm^{-1} (9100 $M^{-1}cm^{-1}$).

Valence-detrapping behavior in solution: The ^{1}H NMR spectrum of **2** in $[D_7]$DMF at 20°C exhibits broad resonances at $\delta = 7.91$ and 6.20 ppm, while that at 70°C exhibits sharp resonances at $\delta = 7.81$ and 6.13 ppm in a 2:1 intensity ratio, indicating that all of the pyrazolate ligands are equivalent on the NMR timescale in solution at this temperature. The variable-temperature NMR studies between −60 and +70°C disclosed the fluxional behavior of **2** in DMF, as discussed below (Figure 3). Each sharp resonance at 70°C broadened with decreasing temperature, and the coalescence occurred at 10°C. After the coalescence, the resonance sharpened again with decreasing temperature and split into two distinct resonances, for which each intensity ratio was 2:1. The dynamic behavior was fully reversible over the temperature range studied. These observations strongly indicate that complex **2** retains its original structure at low temperature. The HHCOSY spectrum at −50°C enabled us to assign the proton signals of **2**, in which the integral ratio of H_C & H_E

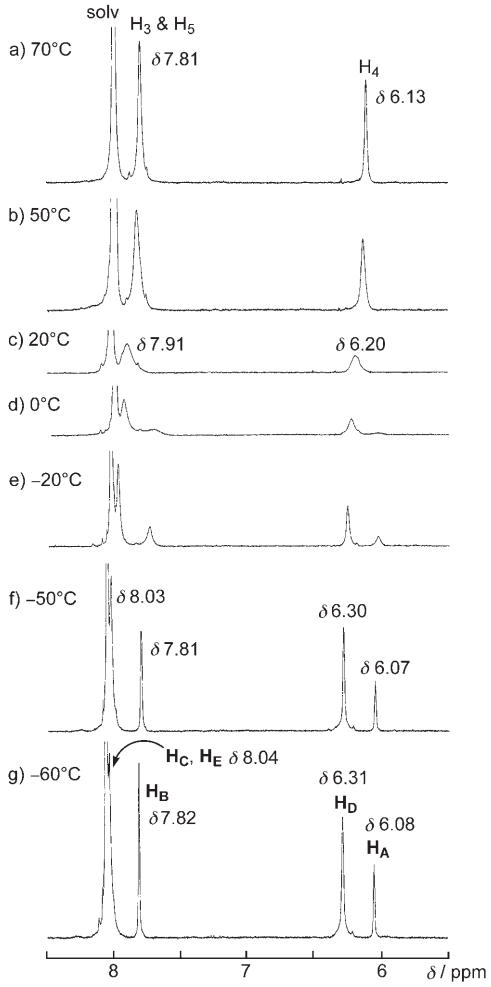

Figure 3. Variable-temperature ^{1}H NMR spectra of **2** in [D_7]DMF.

($\delta = 8.03$ ppm), H_B ($\delta = 7.81$ ppm), H_D ($\delta = 6.30$ ppm) and H_A ($\delta = 6.07$ ppm) is 4:2:2:1 (Scheme 1).

To gain further insight into the dynamic process, the line-broadening kinetics were studied. The simulation of variable-temperature NMR spectra of H_4 signals by the uncoupled two-site exchange model with the population of 0.33 (p_A) and 0.66 (p_B) reproduced well the original spectra, from which the rate constants of each temperature were determined (Figure 4).[20] The activation parameters obtained

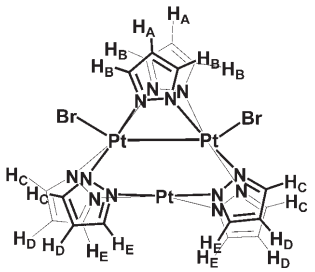

Scheme 1. Schematic representation of **2**. Half of the pyrazolate ligands (black) are related to the rest of ligands (gray) by an idealized mirror plane defined by the three Pt atoms.

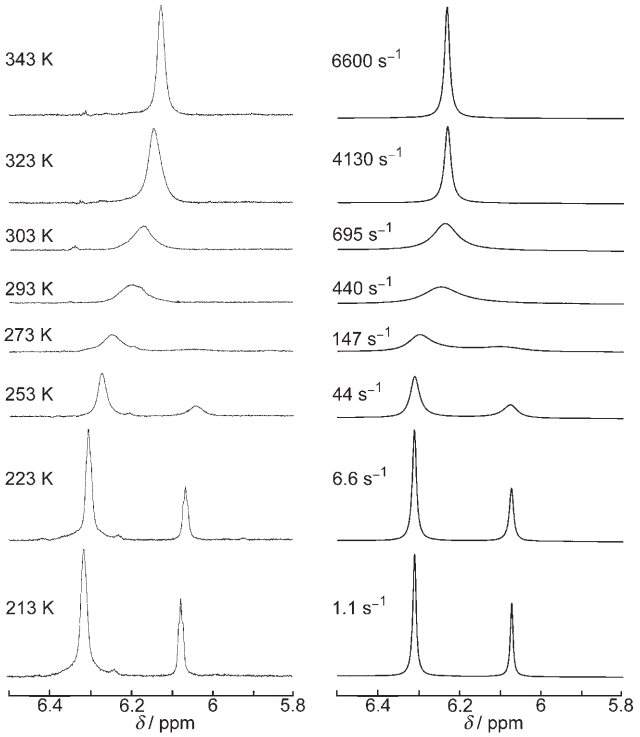

Figure 4. Experimental (left) and simulated (right) variable-temperature ^{1}H NMR spectra of **2** showing the H_4 resonances. Best-fit first-order rate constants ($k_{A\rightarrow B}$) are given with the simulated spectra.

by Eyring analyses were $\Delta H^{\neq} = 37(2)$ kJ mol^{-1} and $\Delta S^{\neq} = -67(7)$ J mol^{-1} K^{-1}. The moderate value of $\Delta H^{\neq}$ indicates that the fluxional behavior occurs easily. The addition of Br^- ions to the solution of **2** in DMF did not have much affect on the UV/Vis spectrum, while the variable-temperature NMR spectra of **2** in the presence of Br^- ions showed a downward shift in the coalescence temperature. These results and the difference in spectrum between **2** and **3** suggest that 1) the two halide anions do not dissociate from Pt atoms, but coordinate with two Pt atoms in DMF, as in the solid-state structure, as an equilibrium structure; 2) one Pt atom is not coordinated with halide anion even when halide anion exists in excess; and 3) the fluxional process occurs in associative manner, maybe, either through the approach of DMF to the Br-coordinated Pt center or approach of Br^- to the uncoordinated Pt atom in the presence of excess Br^- ions. Thus it is concluded that the migration of Br^- ion (i.e., the dissociation of Br^- ion from one of the Pt^{III} centers followed by rebinding of the Br^- ion with the Pt^{II} center) occurs with the concomitant shift of the Pt–Pt bond. This fluxional process is temperature-dependent and corresponds to the valence-detrapping, which can be formally represented in Scheme 2.[16–18,21,22] It is worth noting that the valence-detrapped state may be classified into "Phase III" of the theoretical model, which was constructed for the trinuclear mixed-valence complex $[Fe_3(\mu\text{-}O)(\mu\text{-}O_2CCH_3)_6(py)_3]\cdot(py)$ to explain the observed temperature dependencies of heat capacity and Mössbauer spectra.

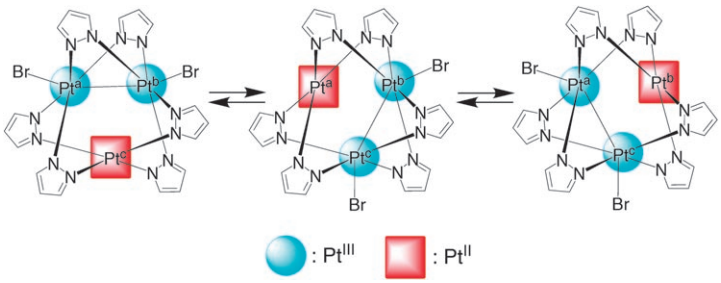

Scheme 2. Fluxional behavior of **2** due to valence-detrapping showing the migration of Br^- ion and the concomitant shift of the Pt–Pt bond.

As described below, an intense band at 30600 cm^{-1} (band C) in the UV/Vis spectrum of **2** is assigned to the intervalence charge-transfer (IVCT) excitation. The thermal electron-transfer energy ($E_{th}^{\neq}$) is expected to be 1/4 of IVCT transition energy according to Hush model;[21] $E_{th}^{\neq} = E_{op}/4 =$ 7650 cm^{-1} (91.5 kJ mol^{-1}). However, the activation enthalpy ($\Delta H^{\neq}$), observed for the fluxional behavior of **2**, which corresponds to the electron transfer, is smaller than the 1/4 of the IVCT excitation energy. This is not surprising, because the IVCT excitation occurs without the movement of Br^- ion, and, maybe, the coordination of DMF due to Franck-Condon principle, but the thermal electron transfer occurs with the Br^- movement and the DMF coordination (see Supporting Information "Relationship between IVCT band and $\Delta H^{\neq}$ value of fluxional behavior").

Electronic structure: To understand the electronic structures of pyrazolato-bridged $Pt_3^{II,III,III}$ complexes, $[Pt_3Br_2(\mu\text{-}pz)_6]$ (**2**) and its chloro analogue **3** were investigated by DFT methods. The fundamental geometrical features of **2** are well reproduced by the DFT calculations. The largest deviation between experimental and theoretical bond lengths is in the Pt1–Pt1* distance; the calculated value is longer than the experimental value by 0.096 Å (Table S3 in the Supporting Information). Several molecular orbitals important to the band assignments and the Pt–Pt bond are shown in Figure 5.[23] Evidently the HOMO (MO 167) mainly consists of the d_σ–d_σ bonding overlap between Pt1 and Pt1* atoms and the d_σ–p_σ antibonding overlap between Pt1 (or Pt1*) and Br, into which the d_{z^2} orbital of Pt2 mixes in an antibonding way with the d_σ–d_σ bonding overlap. The LUMO (MO 168) involves the d_σ–p_σ antibonding overlap between Pt1 (or Pt1*) and Br and the antibonding overlap of two d_σ orbitals between Pt1 and Pt1*, into which the d_{z^2} orbital of Pt2 does not mix at all, because of the difference in symmetry. The rest of the lower energy molecular orbitals consist of the d_{z^2} orbital of Pt2 and the p_σ orbital of Br^- ion (MO 150), the p orbital of bridging ligand (MO 154), the p_π orbital of Br^- ion (MO 158), the p_π orbital of Br^- ion and the d_δ orbital of Pt1 and Pt1* (MO 165), and the d_π orbital of Pt2 (MO 166). Essentially the same orbitals are observed in the chloro analogue **3**. Electronic excitation energies calculated by the time-dependent (TD) DFT (B3LYP) method are somewhat smaller than the experimental values as shown in Table 1, probably because the DFT calculation does not incorporate well the mixing of the $(d_\sigma\text{–}d_\sigma)\rightarrow(d_\sigma\text{–}d_\sigma)^*$ excited configuration in the $^1A_1$ ground state,[24] in which $(d_\sigma\text{–}d_\sigma)$ and $(d_\sigma\text{–}d_\sigma)^*$ represent d_σ–d_σ bonding orbital and its antibonding counterpart, respectively. To estimate the effects of the participation, the electronic excitation energies by the TD-B3LYP method were corrected by incorporating the differences in the $^1A_1\rightarrow{}^3B_2$ vertical transition energies between the TD-B3LYP and MRMP2 methods (Table S7 in the Supporting Information).[25] The corrected excitation energies for **2** (Table 1) agree well with the observed values. Also, upon going to **3** from **2**, the observed blue shift of each absorption band (1300–2200 cm^{-1}) is in good agreement with the differences of calculated excitation energies between **2** and **3** estimated by TD-DFT calculations (Tables S5 and S6 in the Supporting Information).

The most intense band at 30600 cm^{-1} (band C) with $\varepsilon =$ 9100 $M^{-1}cm^{-1}$ is readily assigned to the intervalence transition from d_{z^2} orbital of Pt^{II} ion to $(d_\sigma\text{–}d_\sigma)^*$ orbital of the Pt1–Pt1* bond (MO 150→MO 168), which exhibits in part LMCT character. The $(d_\sigma\text{–}d_\sigma)\rightarrow(d_\sigma\text{–}d_\sigma)^*$ transition (MO 167→MO 168) moderately contributes to this band. The second band at 21000 cm^{-1} (band B) with $\varepsilon =$ 1800 $M^{-1}cm^{-1}$ is attributed mainly to the LMCT transition (MO 165→MO 168). The $(d_\sigma\text{–}d_\sigma)\rightarrow(d_\sigma\text{–}d_\sigma)^*$ transition (MO 167→MO 168) and intervalence transition (MO 150→MO 168) also contribute to this band to some extent.

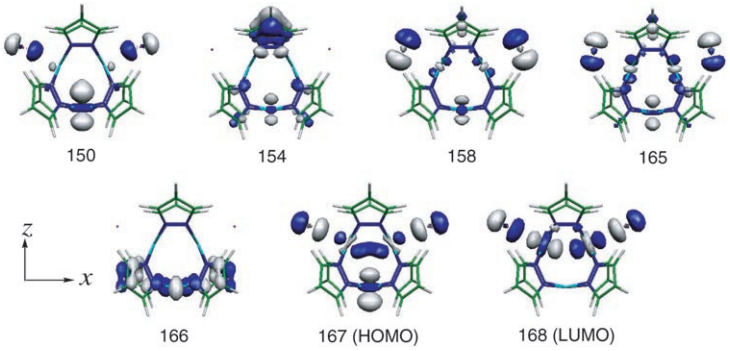

Figure 5. Isosurface plots ($\psi = \pm 0.05$ a.u.) of several molecular orbitals important to the band assignment and Pt–Pt bond for **2** at time-dependent B3LYP method.

The lowest energy band at 16900 cm^{-1} (band A) with $\varepsilon =$ 3400 $M^{-1}cm^{-1}$ mainly consists of the $(d_\sigma\text{–}d_\sigma)\rightarrow(d_\sigma\text{–}d_\sigma)^*$ transition (MO 167→MO 168), in which the LMCT transition (MO 165→MO 168) and intervalence transitions (MO 166→MO 168, MO 150→MO 168) also participate. Thus, the $(d_\sigma\text{–}d_\sigma)\rightarrow(d_\sigma\text{–}d_\sigma)^*$ transition is responsible to the intense deep blue color of **2**, and the influence of the axial ligands on the color (i.e., absorption spec-

Table 1. Calculated and corrected transition energies, oscillator strengths, and band assignments for the electronic absorption spectrum of $[Pt_3Br_2(\mu\text{-}pz)_6]$ (**2**) by the time-dependent B3LYP method with Basis III.[a–c]

Band	Observed position [cm^{-1}]	Calcd position [cm^{-1}] (corrected position)[d] <calcd osc strength>	Assignment transition	coefficient
A	16900	13040 (17840)	167→168	0.45320
		$<f=0.0381>$	165→168	0.29688
			166→168	−0.28415
			150→168	0.19524
B	21000	15720 (20520)	165→168	0.57501
		$<f=0.0351>$	167→168	−0.20990
			150→168	−0.19965
			158→168	0.13052
			154→168	−0.12863
C	30600	27880 (32680)	150→168	0.56679
		$<f=0.5347>$	167→168	−0.14480

[a] Selected optimized geometrical parameters for the $^1A_1$ state of **2** are Pt1−Pt1*, 2.875 (2.7787); Pt1−Pt2, 3.186 (3.1267); Pt1−Br1, 2.667 (2.584); Pt1*-Pt1-Pt2, 63.182 (63.618); Pt1*-Pt1-Br1, 154.570 (156.40); Pt1*-Pt1-N11, 68.053 (69.1/69.4); Pt2-Pt1-N21, 61.991 (62.1/61.8), in which the values in parentheses are experimental data (distances in Å and angles in degree). [b] The transition energies and oscillator strengths calculated with Basis I, II, IV, V and VI are summarized in Tables S5 and S6 in the Supporting Information. [c] Basis III: Pt (LANL2DZ); H, C, N, Br (cc-pVDZ) [d] The electronic structure of the ground state $^1A_1$, which has two main configurations, must be calculated with multiconfigurational method to present correct electronic structure. This means that the DFT-calculated value considerably deviates from the correct value. On the other hand, the excited states, $^3B_2$ and $^1B_2$, can be described well by the TD-DFT method. To estimate the multiconfigurational effects of the ground state, transition energies by the TD-DFT method were corrected by considering the difference in $^1A_1 \rightarrow {}^3B_2$ vertical transition energies between TD-DFT and MRMP2 methods. The correction was made with the following relation; $\Delta E_{correct} = \Delta E(\text{MRMP2}) - \Delta E(\text{TD-B3LYP})$, in which ΔE is $^1A_1 \rightarrow {}^3B_2$ vertical transition energies.

trum) of $Pt_3^{II,III,III}$ complexes is attributed to the contribution of the LMCT character of this transition, because halide p_σ orbital participates in both MO 167 and MO 168. Actually, this band is observed at higher energy in **3**, which is reproduced well by the TD-DFT calculation. Similar assignment was presented for the absorption band at 680 nm in *cis*-diammineplatinum α-pyridone blue (PPB) by SCF-Xα-SW calculations.[26] Usually, the $(d_\sigma\text{–}d_\sigma)\rightarrow(d_\sigma\text{–}d_\sigma)^*$ transition of trivalent platinum dimers appears in the ultraviolet region.[1,3,27] The $(d_\sigma\text{–}d_\sigma)\rightarrow(d_\sigma\text{–}d_\sigma)^*$ transition at the low energy observed here implies that the cyclic trimer structure diminishes the magnitude of the overlap of d_σ orbitals, which leads to the elongation of Pt−Pt bond to raise the energy of $(d_\sigma\text{–}d_\sigma)$ bonding orbital and to lower the energy of $(d_\sigma\text{–}d_\sigma)^*$ antibonding orbital. These are consistent with the facts that the $Pt_3^{II,III,III}$ complexes are sensitive towards light in solution.

Conclusion

Two-electron oxidation of the cyclic trimer consisting of square-planar Pt^{II} ions produces a spin-paired $Pt_3^{II,III,III}$ species with localized Pt−Pt bond rather than $Pt^{8/3}Pt^{8/3}Pt^{8/3}$ species with delocalized Pt−Pt bonds. We have succeeded in the isolation and the first structural characterization of the $Pt_3^{II,III,III}$ species. The theoretical calculations revealed that the HOMO and LUMO of $Pt_3^{II,III,III}$ species mainly consist of $(d_\sigma\text{–}d_\sigma)$ and $(d_\sigma\text{–}d_\sigma)^*$ orbitals, respectively, and the origin of deep blue color of the bromo complex, **2**, arises from the $(d_\sigma\text{–}d_\sigma)\rightarrow(d_\sigma\text{–}d_\sigma)^*$ transition. Unique fluxional behavior in DMF was analyzed by variable-temperature NMR studies. This fluxional behavior is reasonably attributed to valence-detrapping, which occurs through the migration and rebinding of Br^- ion with the concomitant shift of Pt−Pt bond.

Experimental Section

Materials: $[Pt_3(\mu\text{-}pz)_6]$ (**1**) was prepared by literature methods.[14] All other commercially available reagents were used as purchased.

General: UV/Vis spectra were recorded on a Jasco V-560 spectrophotometer at 20 °C. The ^1H NMR spectra including variable-temperature NMR spectra and a 2D spectrum were obtained at 400 MHz with a JEOL JNM-AL400 spectrometer.

Synthesis of $[Pt_3Br_2(\mu\text{-}pz)_6]$ (2): An aqueous solution of $(NH_4)_2Ce(NO_3)_6$ (340 mg, 0.62 mmol/50 mL) was added slowly to a suspension of **1** (292 mg, 0.30 mmol) and KBr (88 mg, 0.74 mmol) in CH_2Cl_2 (200 mL) and the resulting mixture was stirred for 30 min at an ambient temperature. The organic layer was separated, concentrated to 5 mL, and then cooled in a refrigerator over night to complete the precipitation of product. The solid was filtered, washed with diethyl ether, and dried in vacuo. Yield 86 mg, 25%; elemental analysis (%) calcd for $C_{18}H_{18}Br_2N_{12}Pt_3$: C 18.84, H 1.58, N 14.65, Br 13.93; found: C 18.90, H 1.77, N 14.33, Br 13.81; UV/Vis (DMF): $\lambda_{max}(\varepsilon) = 327$ (9100), 475 (1800), 590 nm (3400 $mol^{-1}\,dm^3\,cm^{-1}$); ^1H NMR (400 MHz, $[D_7]$DMF, −60 °C, TMS): $\delta =$ 8.04 (d, 4H; H_C and H_E), 7.82 (d, 2H; H_B), 6.31 (t, 2H; H_D), 6.08 ppm (t, 1H; H_A).

X-ray structural determinations: Single-crystal X-ray diffraction data were collected on a Quantum CCD area detector coupled with a Rigaku AFC7 diffractometer with graphite monochromated $Mo_{K\alpha}$ radiation ($\lambda =$ 0.71069 Å). Data for **2**: crystal dimensions $0.20\times0.20\times0.20$ mm^3, monoclinic, space group $C2/c$, $a = 9.815(2)$, $b = 15.635(5)$, $c = 16.3668(7)$ Å, $\beta =$ 96.595(1)°, $V = 2495.0(10)$ $Å^3$, $Z = 4$, $T = 297$ K, $\rho_{calcd} = 3.055$ $g\,cm^{-3}$, $2\theta_{max} = 55.09$ °, $\mu(Mo_{K\alpha}) = 19.959$ mm^{-1}, symmetry-related absorption correction (transmission coefficient: 0.0079, 0.0185). Reflections: 10656 collected, 2837 unique ($R_{int} = 0.035$), 2356 observed [$I > 2\sigma(I)$]; 159 parameters refined with $R = 0.0328$ [$I > 2\sigma(I)$], w$R_2 = 0.0862$ (all data), GOF = 1.050, residual electron density: +2.42, −1.93 e $Å^{-3}$. The crystal structure was solved by direct method by using SIR92.[28] The positional and thermal parameters of non-hydrogen atoms were refined anisotropically by the full-matrix least-squares method. All calculations were performed using TEXSAN.[29] CCDC-255774 contains the supplementary crystallographic data for this paper. These data can be obtained free of charge from The Cambridge Crystallographic Data Centre via www.ccdc.cam.ac.uk/data_request/cif.

Computational methods: The geometries of $[Pt_3X_2(\mu\text{-}pz)_6]$ (X = Br, Cl) were optimized with the DFT method and the transition energies were evaluated with the time-dependent (TD) DFT method, in which B3LYP functional was employed.[30] In these calculations, various basis set systems (Basis I, II, III, IV, V, and VI) were used. For Pt, the usual LANL2DZ basis set[31] was employed in Basis I–III, and a (311111/22111/411) basis set was used with Stuttgart–Dresden–Bonn effective core potentials (ECPs)[32] in Basis IV, a (541/541/111/1) basis set[31,33] was used with the same ECPs as those of LANL2DZ in Basis V, and a (541/5511/211) basis set was used with ECPs proposed by Christiansen et al.[34] in Basis VI. For Cl and Br, usual LANL2DZ basis sets[35] were used in Basis I, 6–31G basis sets[36] were used in Basis II, cc-pVDZ basis sets[37] were used in Basis III–VI. For C, N, and H atoms, usual 6–31G basis

sets[38] were used in Basis I and II, and cc-pVDZ basis sets[39] were employed in Basis III–VI.

To make correction of the transition energies of the B3LYP method, the MRMP2[40] method was applied to the ground $^1A_1$ state and the excited $^3B_2$ state of these complexes. In the MRMP2 calculations, the CASSCF active space was employed as the reference space, while the 5s and 5p orbitals on Pt atoms, the Ar core orbitals on Br atoms, the Ne core orbitals on Cl atoms, and the 1s orbitals on C and N atoms were kept doubly occupied. The CASSCF active space consists of the Pt1−Pt1* bonding orbital (d_σ–d_σ) and the Pt1−Pt1* antibonding orbital (d_σ–d_σ)*. The B3LYP and MRMP2 calculations were carried out using the Gaussian 98[41] and GAMESS[42] packages, respectively.

Geometry optimization was carried out with Basis I to Basis VI. The agreement with the experimental results becomes better upon going to Basis VI from Basis I, though the differences between Basis I and Basis VI are not large (Supporting Information Tables S3 and S4). The transition energies were evaluated with Basis I to Basis VI. In addition significant differences in the transition energies were not observed between Basis I and Basis VI (Supporting Information Table S5). The MRMP2 calculation was carried out with Basis III, because MRMP2 calculation could not be performed with Basis IV to Basis VI due to the large size of this molecule. In the text, computational results with Basis III are presented, while results with the other basis set systems are presented in the Supporting Information.

Acknowledgements

This work was supported by a Grant-in-Aid for Scientific Research. The authors are grateful to Dr. Makoto Wakeshima and Prof. Yukio Hinatsu at Hokkaido University for the magnetic measurements. We are also grateful to Prof. Masaaki Abe at Kyushu University for valuable discussions.

[1] K. Umakoshi, Y. Sasaki, *Adv. Inorg. Chem.* **1994**, *40*, 187–239.
[2] J. D. Woollins, P. F. Kelly, *Coord. Chem. Rev.* **1985**, *65*, 115–140.
[3] D. M. Roundhill, H. B. Gray, C.-M. Che, *Acc. Chem. Res.* **1989**, *22*, 55–61.
[4] G. Natile, F. P. Intini, C. Pacifico *in Cisplatin* (Ed.: B. Lippert), Verlag Helvetica Chimica Acta, Zürich, **1999**, pp. 429–453.
[5] K. Matsumoto, K. Sakai, *Adv. Inorg. Chem.* **2000**, *49*, 375–427.
[6] K. Matsumoto, M. Ochiai, *Coord. Chem. Rev.* **2002**, *231*, 229–238.
[7] B. Lippert *in Cisplatin* (Ed.: B. Lippert), Verlag Helvetica Chimica Acta, Zürich, **1999**, pp. 379–403.
[8] J. M. Williams, *Adv. Inorg. Chem. Radiochem.* **1983**, *26*, 235–268.
[9] R. J. H. Clark, *Chem. Soc. Rev.* **1990**, *19*, 107–131.
[10] T. Yamaguchi, T. Ito, *Adv. Inorg. Chem.* **2001**, *52*, 205–248.
[11] a) R. J. Cross, *in Comprehensive Organometallic Chemistry II, Vol. 9* (Eds.: E. W. Abel, F. G. A. Stone, G. Wilkinson), Pergamon, Oxford, **1995**, pp. 391–430; b) R. B. King, *Inorg. Chim. Acta* **2003**, *350*, 126–130; c) A. D. Burrows, D. M. P. Mingos, *Coord. Chem. Rev.* **1996**, *154*, 19–69; d) T. Tanase, H. Ukaji, H. Takahata, H. Toda, T. Igoshi, Y. Yamamoto, *Organometallics* **1998**, *17*, 196–209; e) T. Zhang, M. Drouin, P. D. Harvey, *Inorg. Chem.* **1999**, *38*, 957–963; f) R. Bender, P. Braunstein, S.-E. Bouaoud, N. Merabet, D. Rouag, P. Zanello, M. Fontani, *New J. Chem.* **1999**, *23*, 1045–1047; g) K. Osakada, M. Tanabe, T. Tanase, *Angew. Chem.* **2000**, *112*, 4219–4221; *Angew. Chem. Int. Ed.* **2000**, *39*, 4053–4055; h) R. Bender, P. Braunstein, A. Dedieu, P. D. Ellis, B. Huggins, P. D. Harvey, E. Sappa, A. Tiripicchio, *Inorg. Chem.* **1996**, *35*, 1223–1234.
[12] H. Kunkely, A. Vogler, *Chem. Phys. Lett.* **1999**, *308*, 169–172.
[13] a) A. C. Skapski, M. L. Smart, *J. Chem. Soc. Chem. Commun.* **1970**, 658–659; b) N. N. Lyalina, S. V. Dargina, A. N. Sobolev, T. M. Buslaeva, I. P. Romm, *Koord. Khim.* **1993**, *19*, 57–63.
[14] W. Burger, J. Strähle, *Z. Anorg. Allg. Chem.* **1985**, *529*, 111–117.
[15] K. Umakoshi, Y. Yamauchi, K. Nakamiya, T. Kojima, M. Yamasaki, H. Kawano, M. Onishi, *Inorg. Chem.* **2003**, *42*, 3907–3916.
[16] S. E. Woehler, R. J. Wittebort, S.-M. Oh, D. N. Hendrickson, D. Inniss, C. E. Strouse, *J. Am. Chem. Soc.* **1986**, *108*, 2938–2946.
[17] a) S. E. Woehler, R. J. Wittebort, S.-M. Oh, T. Kambara, D. N. Hendrickson, D. Inniss, C. E. Strouse, *J. Am. Chem. Soc.* **1987**, *109*, 1063–1072; b) S.-M. Oh, S. R. Wilson, D. N. Hendrickson, S. E. Woehler, R. J. Wittebort, D. Inniss, C. E. Strouse, *J. Am. Chem. Soc.* **1987**, *109*, 1073–1090.
[18] a) H. G. Jang, S. J. Geib, Y. Kaneko, M. Nakano, M. Sorai, A. L. Rheingold, B. Montez, D. N. Hendrickson, *J. Am. Chem. Soc.* **1989**, *111*, 173–186; b) J. K. McCusker, H. G. Jang, M. Zvagulis, W. Ley, H. G. Drickamer, D. N. Hendrickson, *Inorg. Chem.* **1991**, *30*, 1985–1990; c) C.-C. Wu, H. G. Jang, A. L. Rheingold, P. Gütlich, D. N. Hendrickson, *Inorg. Chem.* **1996**, *35*, 4137–4147.
[19] T. Kambara, D. N. Hendrickson, M. Sorai, S.-M. Oh, *J. Chem. Phys.* **1986**, *85*, 2895–2909.
[20] J. Sandström, *Dynamic NMR Spectroscopy*, Academic Press, London, **1982**.
[21] R. D. Cannon, R. P. White, *Prog. Inorg. Chem.* **1988**, *36*, 195–298.
[22] a) C.-C. Wu, S. A. Hunt, P. K. Gantzel, P. Gütlich, D. N. Hendrickson, *Inorg. Chem.* **1997**, *36*, 4717–4733; b) T. Nakamoto, M. Hanaya, M. Katada, K. Endo, S. Kitagawa, H. Sano, *Inorg. Chem.* **1997**, *36*, 4347–4359.
[23] P. Flukiger, H. P. Luthi, S. Portmann, J. Weber, MOLEKEL 4.0, Swiss Center for Scientific Computing, Manno, Switzerland, **2000**.
[24] The $^1A_1$ ground state is calculated to be somewhat less stable due to insufficient incorporation of the excited configuration from the (d_σ–d_σ) bonding orbital to its antibonding counterpart.
[25] Because the MRMP2 calculation of the singlet-excited state is difficult, we calculated the $^1A_1 \rightarrow {}^3B_2$ excitation energy with TD-DFT and MRMP2 methods. The difference in this excitation energy between TD-DFT and MRMP2 methods roughly corresponds to the underestimation of the energy of the $^1A_1$ ground state by the DFT method, because the $^3B_2$ state is little influenced by the mixing of the (d_σ–d_σ)→(d_σ–d_σ)* excited configuration.
[26] A. P. Ginsberg, T. V. O'Halloran, P. E. Fanwick, L. S. Hollis, S. J. Lippard, *J. Am. Chem. Soc.* **1984**, *106*, 5430–5439.
[27] a) R. A. Newman, D. S. Martin, R. F. Dallinger, W. H. Woodruff, A. E. Stiegman, C.-M. Che, W. P. Schaefer, V. M. Miskowski, H. B. Gray, *Inorg. Chem.* **1991**, *30*, 4647–4654; b) C.-M. Che, W.-M. Lee, K. C. Cho, *J. Am. Chem. Soc.* **1988**, *110*, 5407–5411; c) C.-M. Che, T. C. W. Mak, V. M. Miskowski, H. B. Gray, *J. Am. Chem. Soc.* **1986**, *108*, 7840–7841; d) R. Stranger, S. C. Nissen, M. T. Mathieson, T. G. Appleton, *Inorg. Chem.* **1997**, *36*, 937–939.
[28] A. Altomare, G. Cascarano, C. Giacovazzo, A. Guagliardi, M. C. Burla, G. Polidori, M. Camalli, *J. Appl. Crystallogr.* **1994**, *27*, 435–436.
[29] teXsan: Crystal Structure Analysis Package, Molecular Structure Corporation, The Woodlands, TX 77381, USA, **1999**.
[30] a) A. D. Becke, *J. Chem. Phys.* **1992**, *96*, 2155–2160; b) A. D. Becke, *J. Chem. Phys.* **1993**, *98*, 5648–5652; c) C. Lee, W. Yang, R. G. Parr, *Phys. Rev. B* **1988**, *37*, 785–789.
[31] P. J. Hay, W. R. Wadt, *J. Chem. Phys.* **1985**, *82*, 299–310.
[32] D. Andrae, U. Häußermann, M. Dolg, H. Stoll, H. Preuß, *Theor. Chim. Acta* **1990**, *77*, 123–141.
[33] a) M. Couty, M. B. Hall, *J. Comput. Chem.* **1996**, *17*, 1359–1370; b) A. Höllwarth, M. Böhme, S. Dapprich, A. W. Ehlers, A. Gobbi, V. Jonas, K. F. Köhler, R. Stegmann, A. Veldkamp, G. Frenking, *Chem. Phys. Lett.* **1993**, *208*, 237–240.
[34] R. B. Ross, J. M. Powers, T. Atashroo, W. C. Ermler, L. A. LaJohn, P. A. Christiansen, *J. Chem. Phys.* **1990**, *93*, 6654–6670.
[35] W. R. Wadt, P. J. Hay, *J. Chem. Phys.* **1985**, *82*, 284–298.
[36] A. D. McLean, G. S. Chandler, *J. Chem. Phys.* **1980**, *72*, 5639–5648.
[37] D. E. Woon, T. H. Dunning, Jr., *J. Chem. Phys.* **1993**, *98*, 1358–1371.
[38] T. H. Dunning, Jr., *J. Chem. Phys.* **1989**, *90*, 1007–1023.
[39] W. J. Hehre, R. Ditchfield, J. A. Pople, *J. Chem. Phys.* **1972**, *56*, 2257–2261.

[40] a) K. Hirao, *Chem. Phys. Lett.* **1992**, *190*, 374–380; b) K. Hirao, *Chem. Phys. Lett.* **1992**, *196*, 397–403; c) K. Hirao, *Chem. Phys. Lett.* **1993**, *201*, 59–66; d) K. Hirao, *Int. J. Quantum Chem.* **1992**, *S26*, 517–526; e) H. Nakano, MR2D Ver.2, University of Tokyo, **1995**.

[41] Gaussian 98, Revision A.11.3, M. J. Frisch, G. W. Trucks, H. B. Schlegel, G. E. Scuseria, M. A. Robb, J. R. Cheeseman, V. G. Zakrzewski, J. A. J. Montgomery, R. E. Stratmann, J. C. Burant, S. Dapprich, J. M. Millam, A. D. Daniels, K. N. Kudin, M. C. Strain, O. Farkas, J. Tomasi, V. Barone, M. Cossi, R. Cammi, B. Mennucci, C. Pomelli, C. Adamo, S. Clifford, J. Ochterski, G. A. Petersson, P. Y. Ayala, Q. Cui, K. Morokuma, P. Salvador, J. J. Dannenberg, D. K. Malick, A. D. Rabuck, K. Raghavachari, J. B. Foresman, J. Cioslowski, J. V. Ortiz, A. G. Baboul, B. B. Stefanov, G. Liu, A. Liashenko, P. Piskorz, I. Komaromi, R. Gomperts, R. L. Martin, D. J. Fox, T. Keith, M. A. Al-Laham, C. Y. Peng, A. Nanayakkara, M. Challacombe, P. M. W. Gill, B. Johnson, W. Chen, M. W. Wong, J. L. Andres, C. Gonzalez, M. Head-Gordon, E. S. Replogle, J. A. Pople, Gaussian Inc., Pittsburgh PA, **2001**.

[42] M. W. Schmidt, K. K. Baldridge, J. A. Boatz, S. T. Elbert, M. S. Gordon, J. H. Jensen, S. Koseki, N. Matsunaga, K. A. Nguyen, S. Su, T. L. Windus, M. Dupuis, J. A. J. Montgomery, *J. Comput. Chem.* **1993**, *14*, 1347–1363.

Received: May 9, 2006
Published online: June 26, 2006

